Journal of Materials Chemistry A

Accepted Manuscript

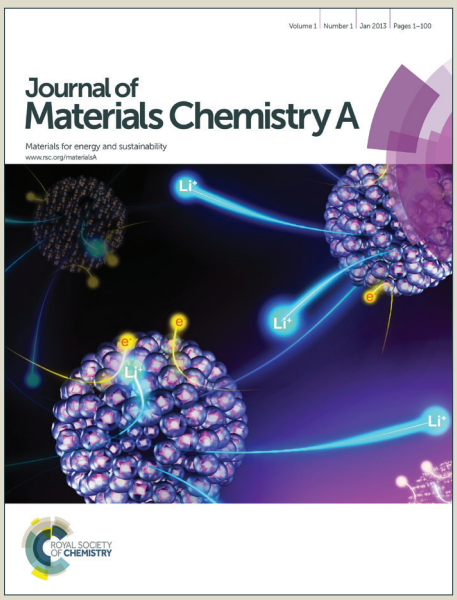

ROYAL SOCIETY OF CHEMISTRY

www.rsc.org/materialsA

Journal of Materials Chemistry A

Journal of Materials Chemistry A

Dynamic Article Links►

Cite this: DOI: 10.1039/c0xx00000x

ARTICLE

www.rsc.org/xxxxxx

A straightforward, eco-friendly and cost-effective approach towards flame retardant epoxy resins

Ionela-Daniela Carja,*[a] Diana Serbezeanu,[a] Tachita Vlad-Bubulac,[a] Corneliu Hamciuc,[a] Adina Coroaba,[a,b] Gabriela Lisa,[c] Celia Guillem López,[d] Mónica Fuensanta Soriano,[d] Vicente Forrat Pérez[d] and Maria Dolores Romero Sánchez[d]

Received (in XXX, XXX) XthXXXXXXXXX 20XX, Accepted Xth XXXXXXXXX 20XX
DOI: 10.1039/b000000x

Modification of epoxy resins with organophosphorus compounds, either as reactive co-reactants or additive, is the key to achieving non-flammable advanced epoxy materials. Herein, through a straightforward and cost-effective approach, epoxy thermosets were prepared by simply mixing a new phosphorus flame retardant (13.5 wt% phosphorus) with a bifunctional bisphenol-A based epoxy polymer, followed by thermal curing in the presence of an aromatic aminic hardener. It was proved that a very low content of phosphorus led to composites exhibiting remarkable improved flame retardancy. 1 wt% phosphorus was enough to increase the limiting oxygen index value with about 30%. Furthermore, the peak of heat release rate was reduced up to 45%, depending on the content of flame retardant additive introduced into the epoxy matrix.The UL-94 V-0 materials were achieved when 2 and 3 wt% phosphorus were added into the epoxy matrix. Thermogravimetric data showed that the incorporation of flame retardant additive significantly increased the char yield and thermal stability of the gradually forming phosphorus-rich carbonaceous layer at elevated temperatures.

Introduction

Epoxy polymers are high performance organic materials which possess reactive oxirane moieties readily available for crosslinking either under catalytic homopolymerization conditions, or in the presence of active hydrogen containing molecules as curing agents, such as polyfunctional amines,[1-3] amides,[4, 5] acids,[6] phenols,[7] thiols[8] etc. Accordingly, infusible thermosets are obtained. These materials are widely used in various areas of electronics, transportation and aerospace industry, as adhesives, composites, paints, protective surface coatings, laminates, encapsulates for semiconductors and electronic devices, due to the low cost, ease of fabrication and to their highly attractive physico-chemical and mechanical characteristics.[9-11] However, as consequence of their elemental composition, which consists mainly from carbon and hydrogen atoms, epoxy resins possess high flammability and low thermal stability at elevated temperatures.[12, 13]

Several strategies are currently employed to improve the flame retardant behaviour of epoxy resins. Notwithstanding that the incorporation of organohalogen containing compounds into epoxy matrices, either as reactive co-reactants or additives, has proven to be an extremely efficient approach,[14] the use of such systems is restricted by the current legislation. The main concern is related to the combustion process itself, which is often accompanied by the release of corrosive or toxic gases, especially, dibenzo-*p*-dioxin and dibenzofuran, and by the production of high amounts of smoke.[15] Therefore, fireproofing, along with recycling and minimum environmental impact, while maintaining the structural integrity of thermosets, are the major challenges for expanding the applications of epoxy resins as high performance materials in various advanced technologies.

The modification of epoxy resins with boron,[16] phosphorus,[17-19] silicon,[20, 21], layered double hydroxides,[22] melamine,[23] montmorilonite[24] etc. has resulted in increased thermal stability and flame retardancy. Among these, the organophosphorus based systems play a crucial role in terms of flame retardant efficiency and low toxicity of the evolved gases during combustion. The phosphorus flame retardant can act either in the condensed phase by altering the rate and/or the pathway of the pyrolytic decomposition mechanism of the fireproof system or, in the gas phase, by scavenging the carrier species which are required to feed the flames. However, it is generally accepted that the phosphorus flame retardants influence the reactions primarily occurring in the condensed phase.[25-31] During the combustion or thermal decomposition, the organophosphorus compound is first transformed into phosphoric acid. Further exposure to the heat causes the formation of non-volatile polyphosphoric acid which reacts with the decomposing polymer by esterification and dehydration to promote the formation of char residue. According to the literature, the formative amount of char yield increases with increasing the phosphorus content added into the polymer.[32-

[34] The char residue acts as a two-way barrier, both shielding the underlying polymer from the attack of the oxygen and radiant heat, enlarging the burning time or extinguishing the fire, and blocking the passage of the combustible gases and molten polymer towards the combustion zone. Thus, the investigation of the decomposition mechanism of phosphorus flame retardants, in order to comprehend the effects of phosphorus concentration on the pyrolysis and flammability of such materials, is a major concern for scientific community.

Recently, 9,10-dihydro-9-oxa-10-phosphaphenanthrene-10-oxide (**DOPO**) has received notable attention from scientists and engineers worldwide due to the multiple structural diversification by functionalization.[35] The active hydrogen of **DOPO** can be reacted with a variety of electron-deficient derivatives, leading to a wide range of compounds with phosphaphenanthrene skeleton. Different low molecular weight **DOPO** containing compounds have been incorporated as additives into epoxy matrices to induce better flame retardant properties. The additivation has the advantages of low manufacturing cost and ease with which these compounds are introduced into polymer matrices. The use of flame retardant additives in order to improve the flame retardant properties of epoxy resins may be a compromise or, in the best case, it may provide the optimal balance of some minimum requirements in different areas of applicability.

Aromatic polyphosphonates as flame-retardant additives are superior to the non-polymeric ones because they possess lower volatility, lower extractability and better compatibility with the base polymers.[36] The general strategy employed to prepare polyphosphonates is based on polycondensation reaction of bisphenols with alkyl(aryl)phosphonic dichlorides. This synthetic procedure includes melt,[37, 38] solution,[39] phase transfer catalyzed reaction[40] and interfacial polycondensation.[41]

In a continuing effort to develop halogen-free flame retardants for practical applications, our laboratory has successfully prepared a series of phosphorus containing polyesters and copolyesters.[42-47] Herein, a new oligophosphonate containing phosphorus both in the main and side chains has been synthesized by solution polycondensation of 1,4-phenylene-bis((6-oxido-6*H*-dibenz[c,e][1,2]oxaphosphorinyl)carbinol) (diol **1**) with phenylphosphonic dichloride (**2**). FTIR and ^{1}H NMR spectroscopy, solubility and molecular weight measurements have been performed to confirm the structure of the new synthesized oligomer. Safe, thermally stable and fire retardant semi-interpenetrating polymer networks (SIPNs), based on the synthesized oligophosphonate and a commercial epoxy resin known as ROPOXID, have been prepared in the presence of 4,4'-diaminodiphenyl methane (**DDM**) as aminic hardener. The performances of the corresponding thermosets in terms of thermal stability and burning behaviour have been studied by differential scanning calorimetry (DSC), thermal gravimetric analysis (TGA), limiting oxygen index (LOI), UL-94 and cone calorimetry measurements. The char residues have been investigated in detail by scanning electron microscopy (SEM) and X-ray photoelectron spectroscopy (XPS).

Experimental

Materials

DOPO was purchased from Chemos GmbH, Germany and dehydrated before use. Terephthaldicarboxaldehyde, **DDM** and phenylphosphonic dichloride (**2**) were provided by Aldrich and used as received. Epoxy resin (DGEBA, commercial name – ROPOXID, with an epoxy equivalent weight (EEW) of 184 – 194 g/equiv) was supplied by POLICOLOR (Romania). All other reagents were used as received from commercial sources or purified by standard methods.

Synthesis of 1,4-phenylene-bis((6-oxido-6H-dibenz[c,e][1,2]oxaphosphorinyl)carbinol) (1)

1,4-Phenylene-bis((6-oxido-6*H*-dibenz[c,e][1,2]oxaphosphorinyl)carbinol) (**1**) was prepared by nucleophilic addition reaction of the active hydrogen of **DOPO** with the carbonyl bond of terephthaldicarboxaldehyde, according to a published procedure.[48] ^{1}H NMR (400 MHz, DMSO–d_6, δ, ppm): 8.33 – 8.10 (m, 4H), 8.04 (m, 1H), 7.90 – 7.48 (m, 2H), 7.62 (m, 1H), 7.53 – 7.11 (m, 12H), 6.45 – 6.25 (m, 2H), 5.45 – 5.10 (m, 2H). FTIR (KBr, thin film, cm^{-1}): 3245 (O–H), 1474 (P–Ar), 1203 (P=O), 935 (P–O–Ar). Anal. calcd. for $C_{32}H_{24}O_6P_2$: C, 67.85; H, 4.27; P, 10.94. Found: C, 67.23; H, 4.32 P, 10.67.

Synthesis of the oligophosphonate PFR

The oligophosphonate **PFR** was obtained by solution polycondensation reaction of equimolecular amounts of **DOPO**-disubstituted diol **1** with phenylphosphonic dichloride, **2**, (Scheme 1) according to the following procedure: In a 500-mL three-neck round-bottom glass flask equipped with a temperature controller, magnetic stirrer and reflux condenser, phenylphosphonic dichloride, **2**, (9.70 g, 50 mmol), diol **1** (28.3 g, 50 mmol) and acetonitrile (200 mL) were mixed at 70 ^{o}C for 1 h. Afterwards, the mixture was gradually heated and refluxed until no HCl emission was observed. The mixture was allowed to cool to the ambient temperature and poured into water, resulting in the formation of a stringy solid. The material was broken up and collected using a Büchner funnel. The whitish amorphous solid was vacuum dried at 60 ^{o}C. Yield: 91%. ^{1}H NMR (400 MHz, DMSO-d_6, δ, ppm): 8.46 – 8.11 (m, 4H), 8.11 – 8.00 (m, 2H), 8.00 – 7.79 (m, 4H), 7.79 –7.26 (m, 10H), 7.26 – 7.00 (m, 5H), 5.97 – 5.19 (m, 2H). FTIR (KBr, cm^{-1}): 2924 (C–H), 1477 (P–Ar), 1205 (P=O), 1044 (P–O–C), 931 (P–O–Ar). Anal. calcd. for $C_{40}H_{33}O_7P_3$: C, 66.27; H, 3.92; P, 13.52. Found: C, 65.99; H, 4.01; P, 13.47.

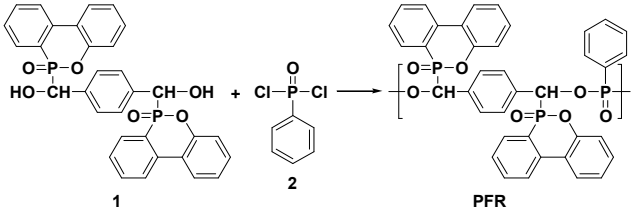

Scheme 1 Synthesis of oligophosphonate **PFR**.

Preparation and curing procedure of phosphorus containing epoxy resins

The **PFR–EP/DDM** SIPNs containing the oligophosphonate **PFR** and ROPOXID – a commercial based DGEBA epoxy resin, denoted as **EP**, were prepared by thermal crosslinking in the presence of **DDM** as curing agent. Various mass ratios of the oligophosphonate **PFR** and **EP** were mixed under continuous stirring at 120 °C. After complete dissolution, the appropriate amount of **DDM** was incorporated into the mixture keeping a **EP** : **DDM** mixing ratio of approximately 3.78 : 1, g : g (this ratio corresponds to an epoxy to amine equivalent of 1 : 1). Afterwards, the mixture was stirred using the mechanical stirrer, until a homogeneous solution was obtained. The reaction mixture was poured into preheated iron molds at 120 ^{o}C and then placed in a vacuum oven at the same temperature for degassing. The modified epoxy resin was subsequently cured in a convection oven at 120 ^{o}C for 2 h and postcured at 130 ^{o}C for 6 h. The samples were slowly cooled to the room temperature to prevent cracking. Scheme 2 shows the schematic representation of the cured networks, as well as the mass ratios between the components.

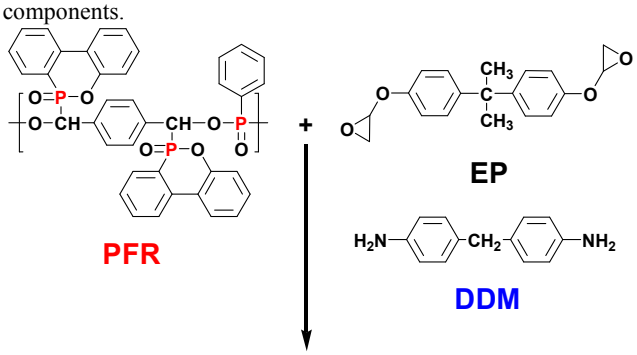

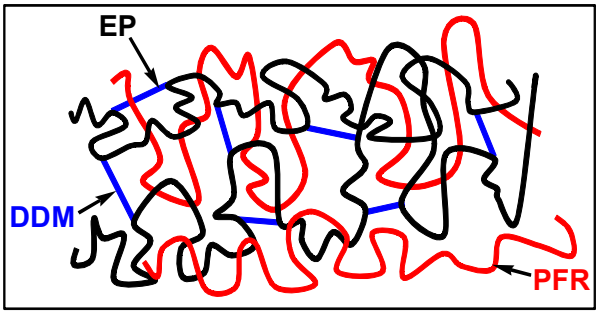

EP/DDM: PFR : EP : DDM = 0 : 3.78 : 1

PFR-EP 1/DDM: PFR : EP : DDM = 0.38 : 3.78 : 1

PFR-EP 2/DDM: PFR : EP : DDM = 0.83 : 3.78 : 1

PFR-EP 3/DDM: PFR : EP : DDM = 1.37 : 3.78 : 1

Scheme 2 Preparation of neat **EP/DDM** system and **PFR–EP/DDM** SIPNs.

Methods

Elemental analysis was carried out with a CHNS 2400 II Perkin Elmer instrument. The phosphorus content was obtained by molybdenum blue method.[49]

FTIR spectroscopy was performed on a Bruker Vertex 70 at frequencies ranging from 4000 to 400 cm^{-1}. Samples were mixed with KBr and pressed into pellets.

^{1}H NMR (400 MHz) spectra were obtained at room temperature on a Bruker Advance DRX spectrometer, using DMSO-d_6 as solvent, and calibrated at 2.512 ppm.

The molecular weights and their distribution were determined by gel permeation chromatography (GPC) with a PL-EMD 950 evaporative mass detector instrument. Two poly(styrene-*co*-divinylbenzene) gel columns (PLgel 5 μm Mixed-D and PLgel 5 μm Mixed-C) were used as stationary phase while *N*,*N*-dimethylformamide (DMF) was the mobile phase. The eluent flow rate was 1.0 mL min^{-1}. Polystyrene standards of known molecular weight were used for calibration.

The inherent viscosity (η_{inh}) was determined at 25 ^{o}C on 0.5% (w/v) **PFR** solution in 1-methyl-2-pyrrolidone (NMP), using an Ubbelohde viscometer.

The glass transition temperature (T_g) of the oligomer and epoxy thermosets in powder form was determined with a Mettler-Toledo differential scanning calorimeter DSC 12 E. Approximately 5 to 8 mg of each sample were encapsulated in aluminium pans having pierced lids to allow the release of volatiles, and run in nitrogen with a heat-cool-heat profile from room temperature up to 250 ^{o}C, at a constant heating rate of 10 ^{o}C min^{-1}. Heat flow *vs.* temperature scans from the second heating run were plotted and the mid-point of inflexion curves was assigned as the T_g of the corresponding sample.

Thermogravimetric analysis (TGA) was carried out under constant nitrogen or air flow (20 mL min^{-1}) at 10 ^{o}Cmin^{-1}, using a Mettler Toledo TGA/SDTA 851^{e} balance. The heating scans were performed on 3 to 5 mg of sample in the temperature range 25 – 700 ^{o}C. Alumina crucible (70 μl) was used as sample holder. To be assured of the data reproducibility, several thermograms have been recorded for each sample.

Scanning electron microscopy (SEM) was performed on a TESLA BS 301 instrument, at 20 kV, with a magnification of 500 – 5000×. The samples were sputtercoated with a conductive layer of gold. The C, N, O and P elements in the residue were verified by the coupled energy dispersive X-ray spectroscope (EDX).

The limiting oxygen index (LOI) values were obtained with an oxygen index instrument Qualitest according to the standard ASTM D2863–09 by measuring the minimum oxygen concentration required to support the candle-like combustion of samples. The test specimens (90 × 6.5 × 3 mm^3) were burned in a precisely controlled atmosphere of nitrogen and oxygen.

Vertical burning test (UL-94) was performed on test specimens (130 × 13 × 3 mm^3) suspended vertically above a cotton patch, used to identify burning droplets. The classifications are defined according to the American National Standard UL 94-2006.

Cone calorimeter measurements were performed on a Fire Testing Technology apparatus equipped with a truncated cone-shaped radiator, at an incident radiant flux of 35 kW m^{-2}, according to the ISO5660 protocol. The test specimens (100 × 100 × 4 mm^3) were placed into the microbalance support which enables the quantification of mass loss evolution during the experiment.

X-ray photoelectron spectroscopy (XPS) was used to determine the chemical composition of the carbonized product which resulted after the thermogravimetric experiments. The XPS spectra were recorded on a KRATOS Axis Nova (Kratos Analytical, Manchester, United Kingdom), using AlKα excitation

radiation with an emission current of 20 mA and a voltage of 15 kV. The base pressure in the sample chamber was maintained between 10^{-8} – 10^{-9} Torr. The incident monochromated X-ray beam was focused on a 0.7 × 0.3 mm^2 area of the surface. Scans were collected over the binding energy -10 – 1200 eV range, using a pass energy of 160 eV with a resolution of 1 eV. The high resolution spectra for all the elements identified from the survey spectra were collected using a pass energy of 40 eV and a step size of 0.1 eV. Data were analyzed using the Vision Processing software (Vision2 software, Version 2.2.10). The binding energy of the C1s peak was calibrated by assuming the binding energy of carbonaceous carbon atom to be 285 eV.

Results and discussion

Synthesis, chemical structure confirmation and general characterization of the oligophosphonate PFR

The oligophosphonate **PFR** contains **DOPO** units linked to the polymer backbone (Scheme 1). Polycondensation reaction of equimolar amounts of **DOPO** disubstituted diol **1** with phenylphosphonic dichloride, **2**, in acetonitrile, yielded **PFR**. The as-synthesized oligomer was isolated by precipitation in water, followed by washing and drying.

The chemical structure of the resulting oligomer was confirmed by elemental analysis, FTIR and ^{1}H NMR spectroscopy. The elemental analysis of **PFR** revealed a slightly lower content in carbon compared to the value theoretically determined as a result of moisture absorption. The oligophosphonate **PFR** showed a strong sharp absorption band at 1477 cm^{-1} due to the aromatic P–C stretching vibrations. The bands appearing at 1205 and 931 cm^{-1} were associated with the aromatic P–O–C stretching vibrations. Aliphatic P–O–C link displayed a strong absorption band at 1044 cm^{-1} due to the asymmetric stretching vibrations. Aromatic P=O stretching bands were found at 1203 cm^{-1}. Important signals were observed at 755 cm^{-1} due to the deformation vibrations caused by the 1,2-disubstituted aromatic **DOPO** rings and at 836 cm^{-1} (deformation vibrations of *p*-phenylene rings).[50] Aromatic C=C stretching bands were found at 1608 and 1508 cm^{-1}. In ^{1}H NMR spectrum of **PFR**, the absence of the multiplet at 6.45 – 6.25 ppm, corresponding to the hydroxil protons, proved the successful synthesis of the proposed structure.

The oligomer **PFR** was highly soluble in polar aprotic solvents such as DMF, *N*,*N*-dimethylacetamide or NMP, as well as in chlorinated hydrocarbon solvents like chloroform or dichloromethane. This good solubility can mainly be explained by the presence of bulky pendant **DOPO** moieties of the diol monomer which increased the free volume and thus facilitated the diffusion of small molecules of solvent among the macromolecules.

GPC was used to obtain the molecular weights and their distribution. The oligophosphonate **PFR** displayed a weight average molecular weight (M_w) of 4562 g/mol and a number average molecular weight (M_n) of 4392 g/mol. The polydispersity M_w/M_n was 1.039. These relative low values of molecular weights can be explained by the incorporation of polar side-chain **DOPO** rings which led to the enhancement in rigidity and polarity of the macromolecules and, consequently, to the decrease of the reactivity at the functional end groups and to the hinder propagation of the polycondensation process.[51] The GPC curve showed narrow molecular weight distribution. It is noteworthy that GPC measurements give rather rough molecular weights than unambiguous values due to the differences in polarity and backbone stiffness between the polystyrene standard and the studied oligomer.

The inherent viscosity of **PFR** was 0.07 dl g^{-1}, value which describes very low molecular weight polymer.

The oligomer **PFR** exhibited moderate glass transition temperature (T_g), around 110 ^{o}C and a tiny melting endotherm centered at 212 ^{o}C, on the considered temperature range, revealing the semi-crystalline behaviour.

TGA performed in nitrogen with 10 °C min^{-1} showed a single-step weight loss for the oligophosphonate **PFR**. The thermogravimetric (TG) and derivative thermogravimetric (DTG) curves are given in Figure 1 (supplementary information). The onset temperature of decomposition (T_{onset}) was around 390 ^{o}C. In the temperature range 390 – 495 ^{o}C, the TG curve was characterized by a sudden weight drop due to the vigorous gas evolution of the underlying sample,with the maximum decomposition temperature around 475 ^{o}C. At temperature above 495 ^{o}C, a relative thermal stable residue was obtained. In air, **PFR** exhibited two main oxidative decomposition steps in the temperature range of 354 – 592 ^{o}C. The first peak mass loss occurred at around 390 ^{o}C, resulting in a mass loss of about 34%. The second peak mass loss occurred at about 574 ^{o}C, with additional materials consumed (~35%) during the oxidation of char. At temperatures above 600 ^{o}C, the mass loss was slightly increased due to the advanced oxidation of char residue. The TG data are listed in Table 1.

The large interval between decomposition and glass transition temperature can be useful for processing this oligomer by thermoforming techniques.

Preparation of the phosphorus containing SIPNs

Due to the low molecular weight and moderate glass transition temperature, **PFR** displayed low melt viscosity such that it could be processed without adding any solubilizer. Consequently, the epoxy SIPNs were prepared by simply mixing the appropriate amount of phosphorus containing additive (**PFR**)into the epoxy matrix (**EP**) at 120 ^{o}C, followed by the addition of **DDM** and thermal treatment at 120 ^{o}C for 2 h and at 130 ^{o}C for 6 h.

FTIR spectroscopy was used to assess the characteristic chemical groups of **PFR** and **EP**, and to verify the formation of diaminodiphenylmethane crosslinks (see Fig. 2 supplementary information). The epoxide ring opening reaction was confirmed by the absence of the characteristic absorption bands of oxirane: a sharp low-to-medium intensity band at 3056 cm^{-1} attributed to the C–H tension of the methylene group of the epoxy ring (stretching vibrations), a strong band at 915 cm^{-1} due to the asymmetric epoxide ring deformation and a strong band centered around 863 cm^{-1} associated to the symmetric epoxide ring deformation.[52-54] These bands dissapeared in the FTIR spectra of the cured samples. Moreover, the peaks at 1172 and at 1225 cm^{-1} characteristic to the secondary and tertiary amines revealed the formation of C–N bonds as a result of the epoxide ring opening reaction with the aromatic diamine.[50] The presence of secondary amine could also suggest that the hardener was not completely consumed in the crosslinking reaction, presumably due to the

reduced mobility of the aromatic diamine molecules and polymeric chains, as result of crosslinking and **PFR** presence which, from this point of view, acted as blocking agent. This assumption is sustained by the increase in intensity of the signal at 1172 cm^{-1} with increasing the **PFR** content. In the IR spectrum of the pristine **EP**, the broad band at 3504 cm^{-1} was assigned to O–H stretching of hydroxyl groups, revealing the presence of dimers or high molecular weight species.[52] The characteristic absorption bands of neat **EP/DDM** systemwerefound at 3400 cm^{-1} (O–H stretching vibrations of unassociated bond in water or phenol and N–H stretching vibrations of secondary amine), 2963 and 2927 cm^{-1} (aliphatic C–H asymmetric stretching vibrations), 2870 cm^{-1} (aliphatic C–H symmetric stretching vibrations), 1610 and 1510 cm^{-1} (aromatic C=C stretching vibrations), 1362 cm^{-1} (C–H deformation vibrations of isopropylidene unit), 1246 and 1035 cm^{-1} (aromatic ether C–O–C asymmetric and symmetric stretching vibrations respectively). **PFR–EP/DDM** SIPNs showed important signals at 3409 cm^{-1}(O–H and N–H stretching vibrations), 2968 and 2879 cm^{-1} (aliphatic C–H stretching vibrations), 1605 and 1515 cm^{-1} (aromatic C=C stretching vibrations), 1474 cm^{-1}(aromatic P–C stretching vibrations), 1363 cm^{-1}(aliphatic C–H deformation vibrations), 1203 cm^{-1} (aromatic P=O stretching vibrations), 1045 cm^{-1} (aliphatic P–O–C stretching vibrations), 930 cm^{-1} (aromatic P–O–C stretching vibrations), 755 cm^{-1} cm^{-1} (deformation vibrations caused by the 1,2-disubstituted aromatic **DOPO** rings) and 716 cm^{-1} (deformation vibrations of the aromatic rings). All these bands confirmed the successful incorporation of **PFR** into the epoxy matrix and the formation of **PFR–EP/DDM** SIPNs.

Compatibility and thermal stability enhancement of phosphorus containing SIPNs

SEM was used to observe the morphology of the fractured samples at low deformation rate. The representative SEM micrographs of the corresponding fracture surfaces of neat **EP/DDM** system and **PFR–EP/DDM** SIPNs (Fig. 1) highlighted the uniform dispersion of the flame retardant additive into the epoxy matrix. The fracture surface of neat **EP/DDM** sample was smooth with low ridges and shallow grooves along the axis of crack growth, specific to the brittle materials. Some small particles were distinguished on the cross section surfaces of **PFR–EP 1/DDM** and **PFR–EP 2/DDM** SIPNs, but these particles were likely resin shards produced during sample fracturing or dust particles. For **PFR–EP 3/DDM** sample, SEM micrograph revealed the existence of microfractures occurring during thermal treatment and initiated by **PFR** agglomerates which acted as stress concentration centers.[55] The fracture surface was rather discontinuous and convoluted, characterized by a feathery texture with large breadth.

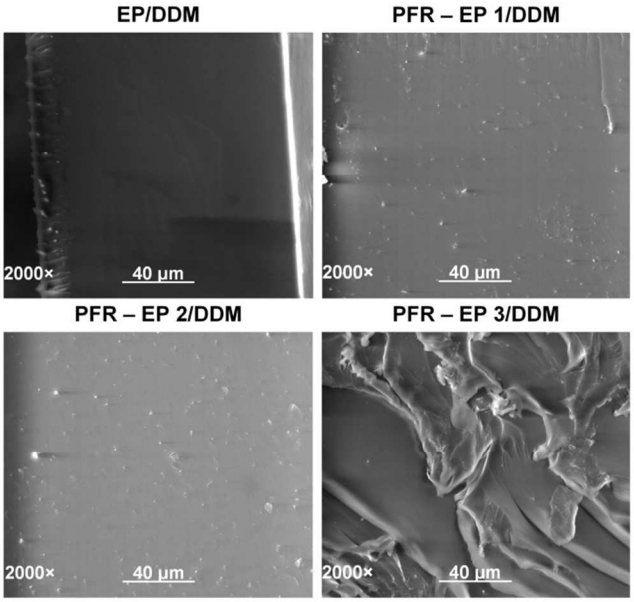

Fig. 1 Representative SEM micrographs of the cross section of neat **EP/DDM** system and **PFR–EP/DDM** SIPNs (SE mode, 20 kV).

The T_gs values of neat **EP/DDM** system and **PFR–EP/DDM** SIPNs were determined by DSC in nitrogen atmosphere at 10 °C min^{-1}. The addition of **PFR** into the epoxy matrix resulted in a homogenuous mixture, with a single glass transition for all **PFR-EP/DDM** SIPNs. The nanodispersion of **PFR** in **EP** is presumed to be the cause for unique T_g, hypothesis sustained by SEM observations. Nevertheless, the miscibility of **PFR-EP** blend, primarily arisen from their polarities, was the key factor to achivieng a good compatibility between the components.

The T_gs values of the cured epoxy resins decreased with increasing the **PFR** content introduced into the epoxy matrix, as it can be observed in Fig. 2. Although the existence of a hindering effect of bulky aromatic **DOPO** units linked to the oligomer backbone on polymer chain motion is not neglected, the almost linear decrease of T_g values with increasing the **PFR** proportion added (Fig. 2 – inset graph), along with the variation of T_g values with the system composition, entitled us to presume that the plasticization effect is the predominant one.[56] To conclude, **PFR** acted like a plasticiser by reducing the crosslinking density and thereby it increased the mobility of molecular chains. In small amount, the addition of the oligomer **PFR** into the epoxy matrix led to a slightly decrease of T_g. Accordingly, the T_g value of **PFR–EP 1/DDM** SIPN was just 2 °C lower than the glass transition corresponding to neat **EP/DDM** system. No exothermic peaks were observed on the DSC curves, suggesting that no further crosslinking reactions have occurred.

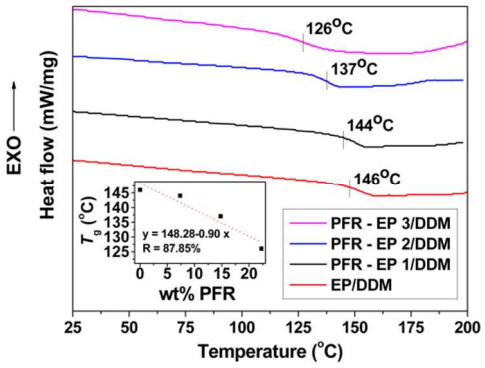

Fig.2 DSC curves of neat **EP/DDM** system and **PFR–EP/DDM** SIPNs.

To investigate the effect of phosphorus content on the thermal stability and decomposition mechanism, it was used TGA carried out under inert atmosphere, as well as in air, with the constant heating rate of 10 °C min^{-1}. The main TG data as determined from the TG and DTG curves are given in Table 1. The moisture absorption was neglected.

Table 1 TG parameters of **PFR**, neat **EP/DDM** system and **PFR–EP/DDM** SIPNs as determined from TG and DTG curves recorded in nitrogen and air atmosphere.

Sample	Nitrogen		Air	
	T_{onset}[1] $\xrightarrow{T_{peak}}$[2] T_{endset}[3], °C (ΔW[4], %)	$\eta_{700°C}$[5] (%)	T_{onset}[1] $\xrightarrow{T_{peak}}$[2] T_{endset}[3], °C (ΔW[4], %)	$\eta_{700°C}$[5] (%)
PFR	$390 \xrightarrow{475} 495$ (49.33)	43.02	$354 \xrightarrow{390} 446$ (34.27); $536 \xrightarrow{574} 592$ (34.52)	23.26
EP/DDM	$350 \xrightarrow{379} 457$ (79.41)	14.7	$275 \xrightarrow{292} 310$ (17.32); $443 \xrightarrow{527} 582$ (79.13)	3.55
PFR–EP 1/DDM	$311 \xrightarrow{371} 535$ (72.51)	26.65	$260 \xrightarrow{285} 310$ (19.04); $433 \xrightarrow{527} 568$ (73.95)	5.02
PFR–EP 2/DDM	$297 \xrightarrow{377} 435$ (71.12)	28.89	$270 \xrightarrow{288} 321$ (21.18); $423 \xrightarrow{527} 575$ (72.99)	5.61
PFR–EP 3/DDM	$304 \xrightarrow{350} 557$ (71.04)	25.74	$261 \xrightarrow{284} 319$ (22.60); $451 \xrightarrow{532} 569$ (68.61)	8.97

[1] onset temperature of polymer decomposition; [2] thermal decomposition peak; [3] thermal decomposition endset temperature; [4] mass loss corresponding to each decomposition stage; [5] char yield measured at 700 °C.

In nitrogen atmosphere, all the samples had a single-step weight loss behaviour, characterized by the emission of high amounts of volatile species (ΔW>68%) with the maximum decomposition temperature above 350 °C. The DTG peak corresponding to the neat cured **EP/DDM** system was slightly shifted to higher temperature when compared to **PFR–EP/DDM** SIPNs, according to the lower thermal stability of the flame retardant additive. However, at elevated temperature, the oligophosphonate **PFR** introduced into the epoxy matrix led to a higher thermal stability of the gradually forming phosphorus-rich carbonaceous layer, as reported in the literature.[57] Therefore, the value of the char yield measured at 700 °C increased about two times in the case of the phosphorus containing samples. Such significant quantity of char could well block the volatilization of the decomposition products, according to the solid phase mechanism of phosphorus flame retardants. Fig. 3 (supplementary information) shows comparatively the TG curves for neat **EP/DDM** system and **PFR–EP/DDM** SIPNs.

TGA measurements performed in air brought relevant information regarding the burning behaviour of neat cured **EP/DDM** system and **PFR–EP/DDM** SIPNs. The presence of oxygen complicated the decomposition mechanism of the cured epoxy resins. Moreover, one additional weight loss was clearly observed at temperatures above 423 °C for neat **EP/DDM** system, as well as for **PFR–EP/DDM** SIPNs. Therefore, the char yields at 700 °C were significantly lower as compared with those obtained in inert atmosphere.

Independently of the atmosphere in which the measurements were performed, the onset temperature and thermal decomposition peak of **PFR–EP/DDM** SIPNs were lower than the ones corresponding to neat **EP/DDM** system, reflecting the high susceptibility to degradation of the P–C bond in the polymer backbone.[48, 58]

To estimate qualitatively the compatibility between the components of the polymer blends, the DTG traces were decomposed in separated curves by using Gaussian profile. It is well known that, if the DTG curves of the blend are simple superpositions of the pure components, the mixture will exhibit low miscibility[59] and, consequently, materials with poor mechanical performances will be obtained. Overlapping of individual profiles such as that of DTG maxima could result in a representation with shoulders, which could be decomposed in separate peak maxima. In Fig. 3, the original DTG curves of neat **EP/DDM** system and **PFR–EP/DDM** SIPNs were decomposed in separated curves by using Gaussian profile. The fitted curve, which was the sum of the separated curves, was consistent with the original DTG trace (with correlation coefficient > 99.98%). The areas of the decomposed peaks (Table 1, supplementary information) were in good agreement with the weight loss (%) values at different stages during thermal degradation. Although

the numbers of decomposition stages of **PFR–EP/DDM** SIPNs decreased, suggesting the simplification in complexity of the degradation mechanism, it could be clearly seen that **PFR** altered the pathway of the pyrolytic decomposition mechanism of the phosphorus containing samples. The additional degradation process in the temperature range 555 – 655 °C observed in the case of neat **EP/DDM** sample was ascribed to the char residue oxidation, less stable than the phosphorus-rich carbonaceous layer obtained for **PFR–EP/DDM** SIPNs.

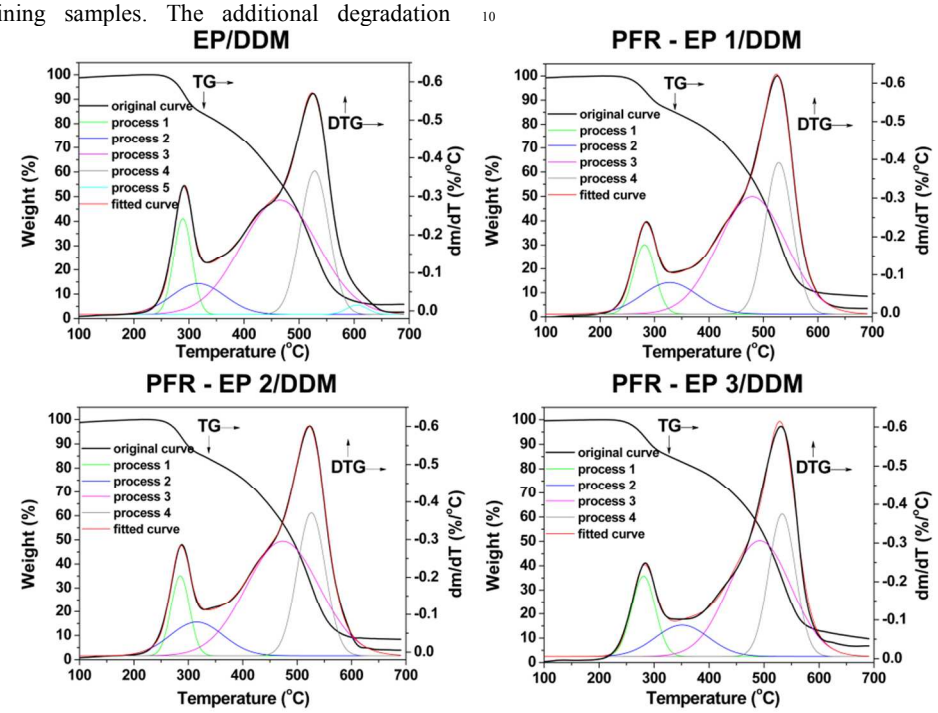

Fig. 3 TG and decomposed DTG curves of neat **EP/DDM** system and **PFR–EP/DDM** SIPNs in air atmosphere.

Flame retardancy of phosphorus containing epoxy SIPNs

Flame retardancy properties of the cured epoxy resins were quantitatively evaluated LOI, UL-94 and cone calorimetry, as shown in Table 2. The LOI values increased linearly with increasing the **PFR** content and reached 42.20%, when 3 wt% phosphorus was added into the system. The results indicate that **PFR** induced good flame retardant effect to epoxy resin. This behaviour is presumed to arise from the high aromaticity of the synthesized phosphorus flame retardant and from the tendency of charring when heated. Indeed, Wang *et all*[48] obtained a LOI value equal to 38.2% for the same phosphorus content added to a similar epoxy system, but using an aliphatic spirocyclic phosphorus containing dichloride derivative, which supports the previous affirmation. Thus, a concentration of 1 wt% phosphorus was enough to increase the LOI value with about 30%. The amount of ash produced after LOI tests was consistent with the TGA results.

Table 2 Phosphorus content and flame retardancy of neat **EP/DDM** system and **PFR–EP/DDM** SIPNs.

Sample	wt P* (%)	wt PFR* (%)	LOI[a] (%)	UL-94	TTI[b] (s)	p-HRR[c] (kWm^{-2})	$t_{p\text{-}HRR}$[d] (s)	THR[e] (MJm^{-2})	$\eta_{600\,^{o}C}$[f] (%)
EP/DDM	0	0	26.49	Not classified	78	275.5	132	56.8	8.6
PFR–EP 1/DDM	1	7.36	34.35	V-1	92	231.7	181	64.8	19.13
PFR–EP 2/DDM	2	14.80	40.05	V-0	80	164.4	197	57.4	24.49
PFR–EP 3/DDM	3	22.28	42.20	V-0	79	150.8	228	46.4	40.33

* theoretically determined; [a] limiting oxygen index; [b] time to ignition; [c] peak of heat release rate; [d] time to reach the peak of heat release rate; [e] total heat release at 1200 s; [f] char yield at 600 °C.

The UL-94 V-0 materials were achieved when 2 and 3 wt% phosphorus were added into the epoxy matrix. These outstanding results indicate that **PFR** imparts excellent flame retardant effect to epoxy resins. The neat **EP/DDM** system showed no UL-94 rating, whereas **PFR–EP 1/DDM** SIPN reached UL 94 V-1 rating of flammability.

Cone calorimetry is a powerful tool to evaluate the combustion behaviour of polymer materials. It provides a comprehensive insight into the fire risks through a series of parameters such as: ease of ignition, flame spread, fire endurance, heat release rate, mass loss rate, ease of extinction, smoke evolution, toxic and corrosive gases release. Table 2 shows the main combustion parameters of the neat **EP/DDM** system and **PFR–EP/DDM** SIPNs: time to ignition (TTI), heat release rate (HRR), peak of heat release rate (p-HRR) total heat release (THR) and char yield at 600 ^{o}C.

As shown in Table 2, **PFR–EP 2/DDM** and **PFR–EP 3/DDM** SIPNs displayed similar TTI values with the control **EP/DDM** system. In the case of **PFR–EP 1/DDM** composition, a significant increase of TTI value was detected. To ignite this material, a higher amount of volatiles is required, which implies rather lower flammability. Based on time to sustained ignition criteria, **PFR–EP 1/DDM** sample could be considered the best candidate for used in various applications. The apparent contradiction with the LOI value obtained for this composition could be explained by the release, upon heating, of more inert gases (like CO_2) and less flammable volatiles, which is advantageous for increasing the TTI value.

Fig. 4 shows the HRR curves of the neat **EP/DDM** system and **PFR–EP/DDM** SIPNs. The **EP/DDM** sample burnt rapidly after ignition and HRR reached a maximum p-HRR value at 275.5 kW m^{-2}. The HRR curves of **PFR–EP 2/DDM** and **PFR–EP 3/DDM** samples exhibited sharp peaks with small shoulders ahead, at low time values (Figure 4, detail). The shape of the HRR curves could be explained by the combustion behaviour of the samples. Under the radiation of 35 kW m^{-2} heat flux, the surface of the samples with higher content of phosphorus, melted and then formed a thin carbonaceous layer which remained intact for a short period of time, corresponding to the appearance of the shoulder. Shortly afterwards, the charred surface was destroyed by the vigorous gas evolution of the underlying sample.

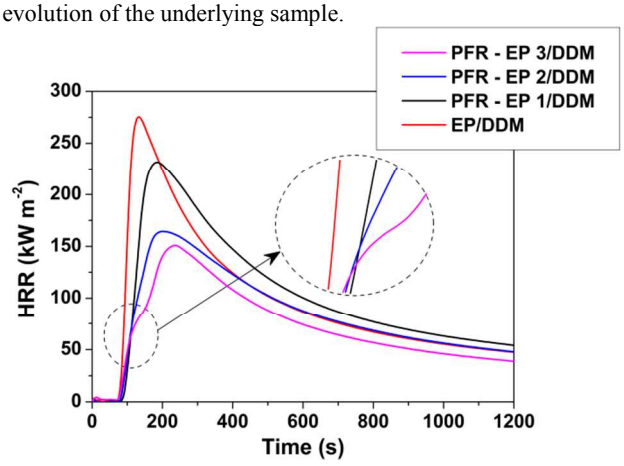

Fig. 4 HRR curves of neat **EP/DDM** system and **PFR–EP/DDM** SIPNs.

The p-HRR values decreased progressively with increasing the amount of **PFR** incorporated into the epoxy matrix. In addition, the p-HRR values of **PFR–EP/DDM** SIPNs were reduced up to 45% of that of neat **EP/DDM** system, depending on the content of the flame retardant additive. This behaviour is typically for the samples with charring tendency.

The $t_{p\text{-HRR}}$ values also increased almost linearly with increasing the **PFR** content (Fig. 4, supplementary information). From practical point of view, this delay implies that there would be more time for escaping during a real fire accident.

As shown in Table 2, the incorporation of **PFR** reduced the heat release capacity and total heat release. The THR value of **PFR–EP 3/DDM** SIPN decreased by 28% when the phosphorus amount introduced into epoxy matrix increased from 1 to 3%.

The increase in char yield with increasing the phosphorus content suggests that the condensed phase mechanism is responsible for the improved flame retardant properties. This hypothesis will be further confirmed by the morphologies and chemistry of the charred layer.

Advanced investigation of structured fire residues and char formation

In order to elucidate how the formation of the phosphorus-rich carbonaceous layer affects the combustion of the cured samples, the residues left after TGA experiments (up to 600 ^{o}C, 10 ^{o}C min^{-1}, air atmosphere) were examined by SEM. Fig. 5 shows the representative SEM micrographs of the corresponding char residues of the neat **EP/DDM** system and **PFR–EP/DDM** SIPNs. The SEM micrograph of the residual char corresponding to the neat **EP/DDM** system revealed a porous and incompact surface, with craters-like holes, formed during the vigorous emission of volatile. By contrast, the phosphorus containing thermosets showed coherent and denser chars than the neat one, shielding the polymer surface from heat and oxygen and, thus, inhibiting the diffusion of the gaseous products towards fire. Furthermore, at higher magnification, the char of **PFR–EP 1/DDM** SIPN (Fig. 5, inset micrograph) revealed some fragile fragments in a non-integral residue structure, corresponding to a slight reduction in p-HRR. **PFR–EP 3/DDM** SIPN, which contains the higher amount of phosphorus, produced the most compacted and integral residue structure (see Fig. 5, inset micrograph), corresponding to the highest reduction in p-HRR.

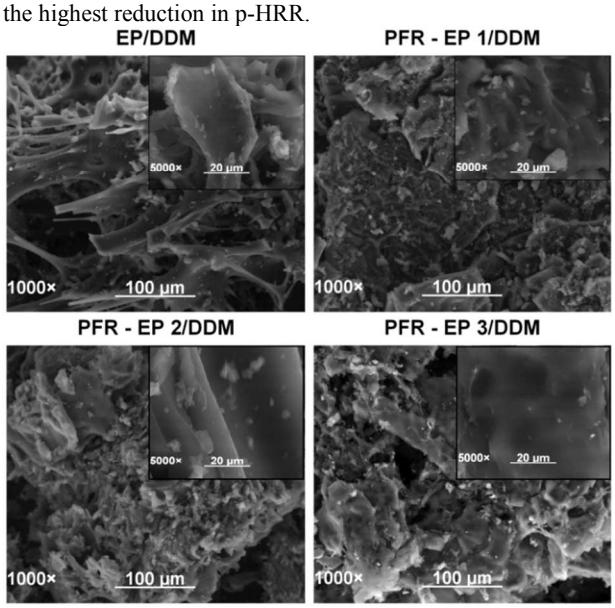

Fig. 5 Representative SEM micrographs of the char residues at 600 ^{o}C of neat **EP/DDM** system and **PFR–EP/DDM** SIPNs (SE mode, 20 kV).

A mapping technique was used to elucidate the atoms distribution onto the char residue surface. The EDX mapping of **PFR–EP 2/DDM** SIPN showed uniform dispersion of phosphorus atoms and a higher concentration of oxygen in the cracks (Fig. 6).

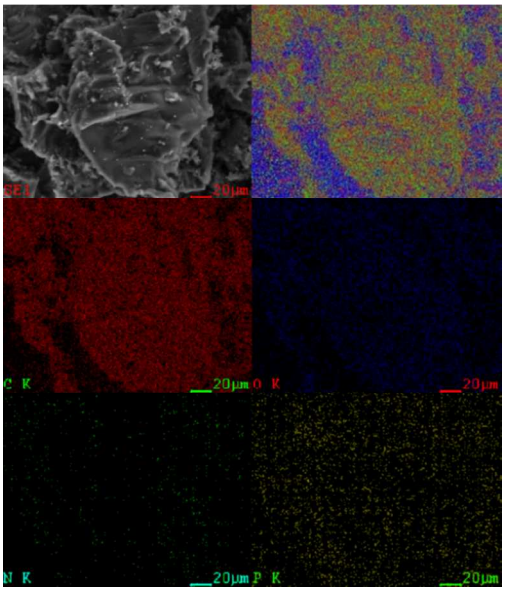

Fig. 6 EDX mapping of the char residue of **PFR–EP 2/DDM** SIPN (SE mode, 20 kV, C: carbon, N: nitrogen, O: oxygen, P: phosphorus).

The semi-quantitative EDX analysis of the char residues confirmed the presence of phosphorus atoms in the char layer. The O/C, N/C and P/C ratios are shown in Fig. 7. The amount of phosphorus (atomic%) in the char residues increased with increasing the content of **PFR** introduced into the epoxy matrix, while the amount of nitrogen decreased as a result of decreasing the crosslinking density, the flame retardant additive acting in this case as a plasticizer. These observations are consistent with FTIR and DSC results. Consequently, the **DDM** molecules that did not entirely participate to the crosslink formation, were more easily removed from the system by volatilization. Chain cleavage firstly occurred at the allylic C–N bond.[60] The concentration of oxygen atoms increased with increasing the amount of phosphorus in the char residue, in agreement with the mechanism of action for the phosphorus derivatives proposed in the literature.[13]

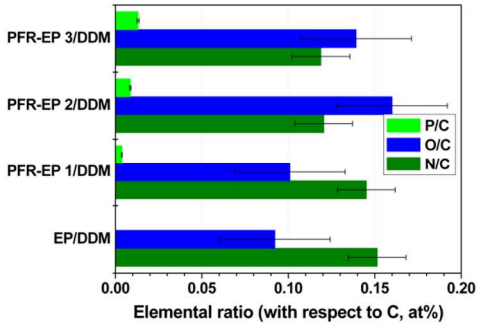

Fig.7 Elemental ratio of O, N and P with respect to C.

XPS is one of the most important methods to perform screening and quantification of a wide range of simple and complex compounds due to its excellent element selectivity and high surface sensitivity. More than that, XPS reflects the atomic scale chemical interactions, i.e. the bonds between neighboring atoms; and thus this method provides reliable structural characteristics for amorphous surface layers of complex composition, for which the application of diffraction techniques is not straightforward.[61] The overall XPS spectra of the char residues corresponding to the neat **EP/DDM** system and **PFR–EP/DDM** SIPNs are given in Fig. 8.

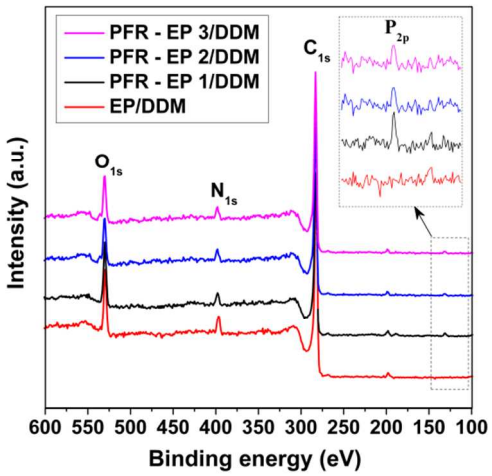

Fig. 8 Overall XPS spectra of the char residues of neat **EP/DDM** system and **PFR–EP/DDM** SIPNs.

The deconvolution of C_{1s}, O_{1s}, N_{1s} and P_{2p} were subsequently recorded to determine precisely the type and content of functional groups. The high resolution C_{1s}, O_{1s}, N_{1s} and P_{2p} spectra of **PFR–EP/DDM** SIPNs were found to be comparable in all types of rigid epoxy polymers with slight differences in relative fraction (atomic%) of different functional groups. Fig. 9 shows comparatively the XPS spectra of C_{1s}, O_{1s}, N_{1s} and P_{2p} of the char residues of neat **EP/DDM** system and **PFR–EP 3/DDM** SIPN. Table 2 (supplementary information) summarizes the surface element concentration as obtained from XPS analysis.

In Fig. 9, the C_{1s} peak of the residue of the pristine cured **EP/DDM** was splitted into five peaks. The peak at 284.6 eV reveals the contribution of C=C in aromatic species in the material, which implies that a graphite-type structure has been formed possibly through dehydration during the combustion.[62] The binding energy of 285 eV can be attributed to C–C or C–H. The peak at around 286.6 eV was assigned to the C–OH or C–N.[63] The signal of C=O bond appeared at 288.3 eV.[63] The signal at 289.9 eV was assigned to COOR groups.[64] The residue of **PFR–EP 3/DDM** SIPN showed an additional peak at 290.8 eV which was assigned to the C–P. In both **EP/DDM** and **PFR–EP 3/DDM** samples, the peak areas assigned to C–C/C=C in aliphatic and aromatic derivative respectively, occupies the overwhelming majority of the C_{1s} peaks, indicating that the carbon is mainly in non-oxidation state, possibly due the fact that carbon, once been oxidized, forms highly volatilized species, such as CO_2, CO and carbonyl compounds.

The XPS spectra of O_{1s} exhibited three peaks at around 530.8 eV (attributed to the double oxygen bond in carbonyl or phosphate units),[65, 66] 532.2 eV (assigned to the simple oxygen bond in C–O–C, C–OH, COOR, C–O–P, P–O–P groups)[67, 68] and 533.2 eV (PhOCOOPh).[66] Due to the presence of organophosphorus compounds in the structure of the residue of **PFR–EP 3/DDM** SIPN, the peak area at of 532.3 eV increased substantially as compared to the one corresponding to the **EP/DDM** residue.

For the N_{1s} spectra, the peaks at around 398.8 eV and 400.5 eV can be attributed to C–N and C=N, respectively.[66] The neat **EP/DDM** system displayed a small peak at 402.3 eV, which could be a result of the formation of quaternary nitrogen and to formation of some oxidized nitrogen compounds, as reported in the literature.[9]

The residual char of **PFR–EP 3/DDM** SIPN revealed the presence of phosphorus containing molecules. The P_{2p} peak was splitted into two peaks. The binding energy of 131.5 eV was assigned to P–O–C or PO_3 groups,[69] while at 132.4 eV appeared the signal of P_2O_5,[70] which was formed during the thermal degradation of phosphorus containing epoxy resin.

The addition of **PFR** strongly influenced the flame retardancy and thermal decomposition of the thermostes. The O/C ratio in the char of **PFR–EP 3/DDM** SIPN increased with about 17% compared to **EP/DDM** system, due to the P atoms which maintain more O atoms, in the form of P(=O)–O into the char. Consequently, lots of P–C, P–O–C, P–O–Ph, P–O–P bonds characteristic to pyrophosphate and polyphosphate type-structures were created in the char of **PFR–EP 3/DDM** SIPN. This means that the incorporation of **PFR** into epoxy matrix promoted the formation of char residue and enhanced the flame retardant properties.

All these data confirm the condensed-phase of **PFR**, by formation, upon decomposition, of polyphosphoric acid which further reacted with the decomposing polymer by esterification and dehydration to promote the formation of a protective phosphorus-rich carbonaceous layer which blocked the mass and energy transport.

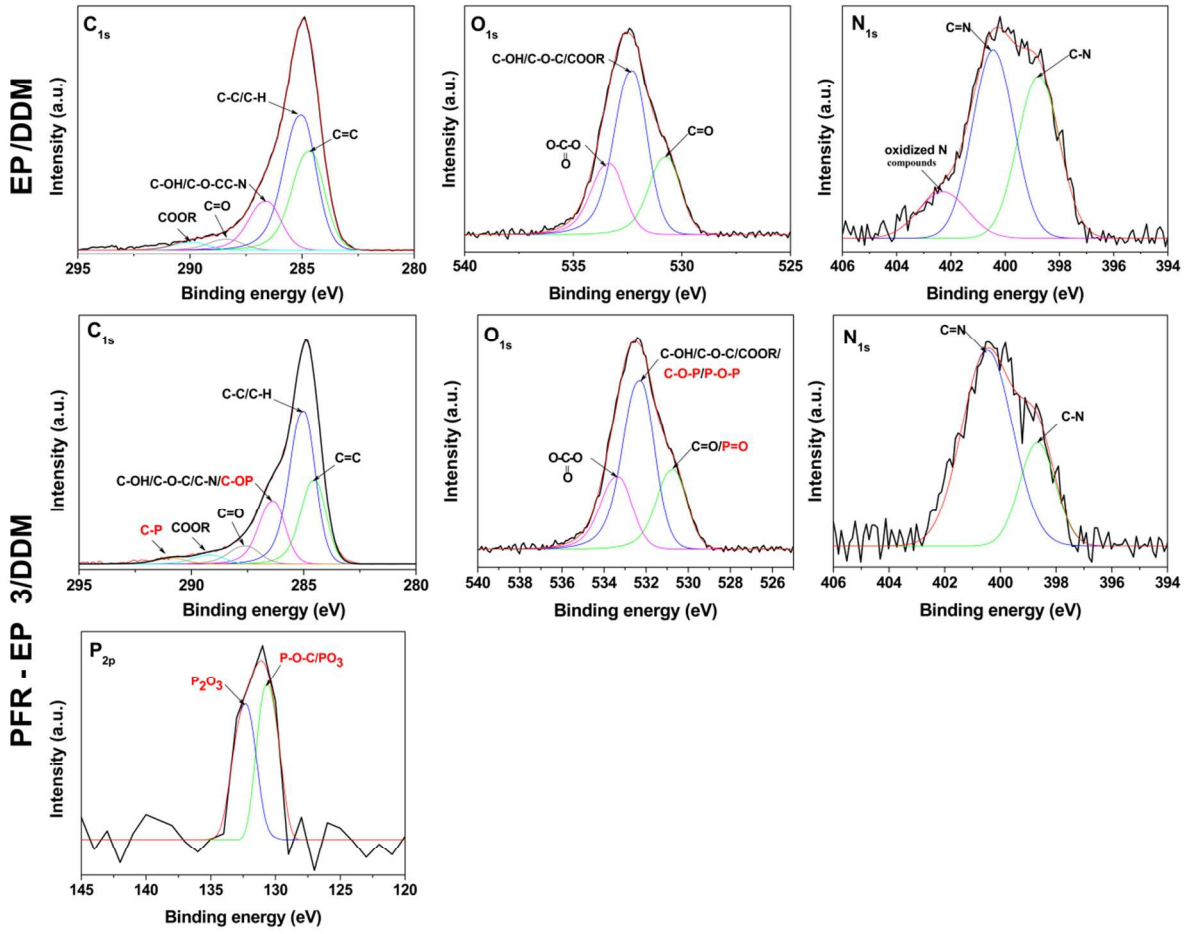

Fig. 9 XPS high resolution scans of **EP/DDM** system and **PFR–EP 3/DDM** SIPN.

Conclusions

A new oligophosphonate containing phosphorus both in the main and side chains was synthesized by solution polycondensation of 1,4-phenylene-bis((6-oxido-6*H*-dibenz[c,e][1,2]oxaphosphorinyl)carbinol) with phenylphosphonic dichloride. Safe, thermally stable and fire retardant SIPNs were prepared by simply mixing the appropriate amount of flame retardant additive with a commercial epoxy resin known as ROPOXID. 4,4'-diaminodiphenyl methane was used as aminic hardener. SEM, DSC and TGA results illustrated good dispersion of phosphorus flame retardant into the epoxy

matrix. Although the addition of the additive led to the early degradation of SIPNs as compared to the neat one, both in oxidative and inert atmosphere, it increased the stability of the residual chars at elevated temperature. It was also shown that with a very low content of phosphorus element, the **PFR–EP/DDM** SIPNs exhibited significantly improved flame retardancy. A concentration of 1 wt% was enough to increase the LOI value with about 30%. In addition, the p-HRR values of the phosphorus containing epoxy thermosets were reduced up to 45% of that of the neat system, depending on the content of the flame retardant additive introduced into the epoxy matrix. These results suggested that the main flame retardancy mechanism of the phosphorus containing epoxy resins was the condensed phase mechanism, hypothesis sustained by SEM and XPS measurements. The epoxy composites formed coherent and denser chars than the neat one. The phosphorus-rich carbonaceous layer prevented the diffusion of the heat and oxygen into the inner layers. Moreover, due to the presence of the phosphine oxide group, which is a very good interacting site in promoting miscibility and adhesion with different substrates, this oligomer could be used as flame retardant agent in various formulations.

Acknowledgements

The financial support offered by CNCSIS-UEFISCDI, project number 28/29.04.2013, code PNII-RU-TE-2012-3-0123 is gratefully acknowledged. Dr. Diana Serbezeanu is thankful to the European Union's Seventh Framework Programme (FP7/2007-2013), under grant agreement n°264115–STREAM, for the financial support offered to investigate the flame retardant properties of the materials. This paper is dedicated to the 65th anniversary of "Petru Poni" Institute of Macromolecular Chemistry of Romanian Academy, Iasi, Romania.

Notes and references

[a] *"Petru Poni" Institute of Macromolecular Chemistry, Aleea Gr. Ghica Vodă 41A, Iaşi-700487, Romania. Fax: +40-232-211299; Tel: +40-232-217454; E-mail: daniela.carja@icmpp.ro*

[b] *Centre of Advance Research in Bionanoconjugates and Biopolymers, Aleea Gr. Ghica Vodă 41A, Iaşi-700487, Romania. Fax: +40-232-211299; Tel: +40-232-217454*

[c] *Faculty of Chemical Engineering and Environmental Protection, "Gheorghe Asachi" Technical University, Bulevardul D. Mangeron 71, Iasi-700050, Romania. Fax: +40-232-271311; Tel: +40-232-278683*

[d] *Technological Institute of Construction Marble Technical Unit (AIDICO), Cami de Castella, 4, 03660 Novelda, Alicante, Spain. Fax: +34-965-608304; Tel: +34-965-608302*

† Electronic Supplementary Information (ESI) available: [Additional experimental details and spectra, including FTIR spectra of the polymers, a figure indicating the thermal stability of the phosphorus flame retardant additive (PFR), a figure indicating thermogravimetric measurements of neat EP/DDM system and PFR – EP/DDM SIPNs (nitrogen atmosphere, 10 °C/min), a figure indicating the variation of time to reach the peak of heat release rate ($t_{p\text{-}HRR}$) on the flame retardant additive (PFR) content, a table showing the areas of the decomposed peaks on the DTG curves for the rigid epoxy polymers, and a table showing the surface element concentration of the residual chars corresponding to the cured samples]. See DOI: 10.1039/b000000x/

1 C. Hamciuc; D. Serbezeanu; I. D. Carja; T. Vlad-Bubulac; V. E. Musteata; V. Forrat Pérez; C. Guillem López; A. López Buendia, *J. Mat. Sci.*, 2013, **48**, 8520-8529.

2 H. Ai; K. Xu; H. Liu; M. C. Chen; X. J. Zhang, *J. Appl. Polym. Sci.*, 2009, **113**, 541-546.

3 Y. C. Chiu; C. C. Huang; H. C. Tsai; A. Prasannan; I. Toyoko, *Polym. Bull.*, 2013, **70**, 1367-1382.

4 P. L. Kuo; J. S. Wang; P. C. Chen; L. W. Chen, *Macromol. Chem. Phys.*, 2001, **202**, 2175-2180.

5 M. Hayaty; H. Honarkar; M. H. Beheshty, *Iran. Polym. J.*, 2013, **22**, 591-598.

6 X. Liu; W. Xin; J. Zhang, *Bioresource Technol.*, 2010, **101**, 2520-2524.

7 S. X. Cai; C. H. Lin, *J. Polym. Sci. A Polym. Chem.*, 2005, **43**, 2862-2873.

8 C. Luo; J. Zuo; J. Zhao, *High Perform. Polym.*, 2013, **25**, 986-991.

9 X. Wang; Y. Hu; L. Song; W. Xing; H. Lu; P. Lv; G. Jie, *Polymer*, 2010, **51**, 2435-2445.

10 W. Zhang; X. Li; R. Yang, *Polym. Degrad. Stab.*, 2011, **96**, 2167-2173.

11 W. Zhang; X. Li; L. Li; R. Yang, *Polym. Degrad. Stab.*, 2012, **97**, 1041-1048.

12 A. Toldy; A. Szabó; C. Novák; J. Madarász; A. Tóth; G. Marosi, *Polym. Degrad. Stab.*, 2008, **93**, 2007-2013.

13 F. Laoutid; L. Bonnaud; M. Alexandre; J. M. Lopez-Cuesta; P. Dubois, *Mater. Sci. Eng. R-Rep.*, 2009, **63**, 100-125.

14 C. H. Lin; S. L. Chang; T. P. Wei; S. H. Ding; W. C. Su, *Polym. Degrad. Stab.*, 2010, **95**, 1167-1176.

15 L. W. D. Weber; H. Greim, *J. Toxicol. Environ. Health* 1997, **50**, 195-215.

16 C. Martín; G. Lligadas; J. C. Ronda; M. Galià; V. Cádiz, *J. Polym. Sci. A Polym. Chem.*, 2006, **44**, 6332-6344.

17 C. H. Lin; T. Y. Hwang; Y. R. Taso; T. L. Lin, *Macromol. Chem. Phys.*, 2007, **208**, 2628-2641.

18 X. Li; Y. Ou; Y. Shi, *Polym. Degrad. Stab.*, 2002, **77**, 383-390.

19 P. M. Hergenrother; C. M. Thompson; J. G. Smith Jr; J. W. Connell; J. A. Hinkley; R. E. Lyon; R. Moulton, *Polymer*, 2005, **46**, 5012-5024.

20 L. A. Mercado; M. Galià; J. A. Reina, *Polym. Degrad. Stab.*, 2006, **91**, 2588-2594.

21 Y. Zheng; K. Chonung; X. Jin; P. Wei; P. Jiang, *J. Appl. Polym. Sci.*, 2008, **107**, 3127-3136.

22 C. H. Tseng; H. B. Hsueh; C. Y. Chen, *Compos. Sci. Technol.*, 2007, **67**, 2350-2362.

23 S. M. Cakić; I. S. Ristić; V. M. Jašo; R. Ž. Radičević; O. Z. Ilić; J. K. B. Simendić, *Prog. Org. Coat.*, 2012, **73**, 415-424.

24 B. Guo; D. Jia; C. Cai, *Eur. Polym. J.*, 2004, **40**, 1743-1748.

25 M. Cochez; M. Ferriol; J. V. Weber; P. Chaudron; N. Oget; J. L. Mieloszynski, *Polym. Degrad. Stab.*, 2000, **70**, 455-462.

26 J. R. Ebdon; D. Price; B. J. Hunt; P. Joseph; F. Gao; G. J. Milnes; L. K. Cunliffe, *Polym. Degrad. Stab.*, 2000, **69**, 267-277.

27 S. Duquesne; J. Lefebvre; G. Seeley; G. Camino; R. Delobel; M. Le Bras, *Polym. Degrad. Stab.*, 2004, **85**, 883-892.

28 Y. Deng; Y. Z. Wang; D. M. Ban; X. H. Liu; Q. Zhou, *J. Anal. Appl. Pyrolysis*, 2006, **76**, 198-202.

29 O. Petreus; G. Lisa; E. Avram; D. Rosu, *J. Appl. Polym. Sci.*, 2011, **120**, 3233-3241.

30 S. Brehme; B. Schartel; J. Goebbels; O. Fischer; D. Pospiech; Y. Bykov; M. Döring, *Polym. Degrad. Stab.*, 2011, **96**, 875-884.

31 V. Benin; S. Durganala; A. B. Morgan, *J. Mater. Chem.*, 2012, **22**, 1180-1190.

32 D. Price; K. Pyrah; T. R. Hull; G. J. Milnes; W. D. Wooley; J. R. Ebdon; B. J. Hunt; C. S. Konkel, *Polym. Int.*, 2000, **49**, 1164-1168.

33 G. H. Hsiue; S. J. Shiao; H. F. Wei; W. J. Kuo; Y. A. Sha, *J. Appl. Polym. Sci.*, 2001, **79**, 342-349.

34 T. S. Leu; C. S. Wang, *J. Appl. Polym. Sci.*, 2004, **92**, 410-417.

35 D. Sun; Y. Yao, *Polym. Degrad. Stab.*, 2011, **96**, 1720-1724.

36 S. Roy; S. Maiti, *Polymer*, 1998, **39**, 3809-3813.

37 O. Petreus; T. Vlad-Bubulac; C. Hamciuc, *Eur. Polym. J.*, 2005, **41**, 2663-2670.

38 S. Percec; A. Natansohn; D. Gâlea; M. Dima, *Angew. Makromol. Chem.*, 1978, **72**, 1-9.

39 O. Petreus; F. Popescu; V. Barboiu; L. Rosescu, *J. Macromol. Sci., Pure Appl. Chem.*, 1988, **25**, 1033-1038.

40 S. Iliescu; A. Pascariu; N. Plesu; A. Popa; L. Macarie; G. Ilia, *Polym. Bull.*, 2009, **63**, 485-495.

41 S. Iliescu; G. Ilia; A. Popa; G. Dehelean; L. Macarie; L. Pacureanu, *Rev. Roum. Chim.*, 2001, **46**, 1041-1046.
42 T. Vlad-Bubulac; C. Hamciuc; O. Petreus; M. Bruma, *Polym. Adv. Technol.*, 2006, **17**, 647-652.
43 T. Vlad-Bubulac; C. Hamciuc, *Polymer*, 2009, **50**, 2220-2227.
44 C. Hamciuc; T. Vlad-Bubulac; O. Petreus; G. Lisa, *Polym. Bull.*, 2008, **60**, 657-664.
45 C. Hamciuc; T. Vlad-Bubulac; I. Sava; O. Petreus, *J. Macromol. Sci., Pure Appl. Chem.*, 2006, **43**, 1355-1364.
46 D. Serbezeanu; T. Vlad-Bubulac; C. Hamciuc; M. Aflori, *J. Polym. Sci. A Polym. Chem.* , 2010, **48**, 5391-5403.
47 I. D. Carja; D. Serbezeanu; T. Vlad-Bubulac; C. Hamciuc; M. Brumă, *Polym. Bull.*, 2012, **68**, 1921-1934.
48 X. Wang; Y. Hu; L. Song; H. Yang; W. Xing; H. Lu, *Prog. Org. Coat.*, 2011, **71**, 72-82.
49 W. Merz, *Mikrochim. Acta*, 1959, **47**, 456-465.
50 G. Socrates, *Infrared and Raman Characteristic Group Frequencies: Tables and Charts, 3rd Edition*. Wiley: Chichester, 2004; p 366.
51 Z. Hu; L. Chen; B. Zhao; Y. Luo; D. Y. Wang; Y. Z. Wang, *Polym. Degrad. Stab.*, 2011, **96**, 320-327.
52 M. González González; J. C. Cabanelas; J. Baselga. 2012. Applications of FTIR on Epoxy Resins - Identification, Monitoring the Curing Process, Phase Separation and Water Uptake. Theophanides, T., Ed. Infrared Spectroscopy - Materials Science, Engineering and Technology. City: InTech. 13, 261-284.
53 G. Nikolic; S. Zlatkovic; M. Cakic; S. Cakic; C. Lacnjevac; Z. Rajic, *Sensors (Basel)*, 2010, **10**, 684–696.
54 H. Siddiqi; A. Afzal; S. Sajid; Z. Akhter, *J. Polym. Res.*, 2013, **20**, 1-10.
55 A. B. Cherian; L. A. Varghese; E. T. Thachil, *Eur. Polym. J.*, 2007, **43**, 1460-1469.
56 C. H. Su; Y. P. Chiu; C. C. Teng; C. L. Chiang, *J. Polym. Res.*, 2010, **17**, 673-681.
57 Y. L. Liu; G. H. Hsiue; R. H. Lee; Y. S. Chiu, *J. Appl. Polym. Sci.*, 1997, **63**, 895-901.
58 X.-G. Ge; C. Wang; Z. Hu; X. Xiang; J.-S. Wang; D.-Y. Wang; C.-P. Liu; Y.-Z. Wang, *J. Polym. Sci. A Polym. Chem.*, 2008, **46**, 2994-3006.
59 C. Vasile; L. Odochian; I. Agherghinei, *J. Polym. Sci. A Polym. Chem.*, 1988, **26**, 1639-1647.
60 U. Braun; A. I. Balabanovich; B. Schartel; U. Knoll; J. Artner; M. Ciesielski; M. Döring; R. Perez; J. K. W. Sandler; V. Altstädt; T. Hoffmann; D. Pospiech, *Polymer*, 2006, **47**, 8495-8508.
61 I. Bertóti, *Surf. Coat. Technol.* , 2002, **151–152**, 194-203.
62 G. Nansé; E. Papirer; P. Fioux; F. Moguet; A. Tressaud, *Carbon*, 1997, **35**, 175-194.
63 Y. Nakayama; F. Soeda; A. Ishitani, *Carbon*, 1990, **28**, 21-26.
64 D. Briggs, *Practical Surface Analysis, Auger and X-ray Photoelectron Spectroscopy, 2nd Edition*. Wiley: Chicheste, New York, 1991; Vol. 1.
65 S. Delpeux; F. Beguin; R. Benoit; R. Erre; N. Manolova; I. Rashkov, *Eur. Polym. J.*, 1998, **34**, 905-915.
66 X. Chen; Y. Hu; C. Jiao; L. Song, *Polym. Degrad. Stab.*, 2007, **92**, 1141-1150.
67 N. M. D. Brown; J. A. Hewitt; B. J. Meenan, *Surf. Interface Anal.*, 1992, **18**, 187-198.
68 P. Y. Shih; S. W. Yung; T. S. Chin, *J. Non-Cryst. Solids* 1998, **224**, 143-152.
69 R. J. J. Jansen; H. van Bekkum, *Carbon*, 1995, **33**, 1021-1027.
70 D. T. Clark; T. Fok; G. G. Roberts; R. W. Sykes, *Thin Solid Films*, 1980, **70**, 261-283.

Graphical Abstract

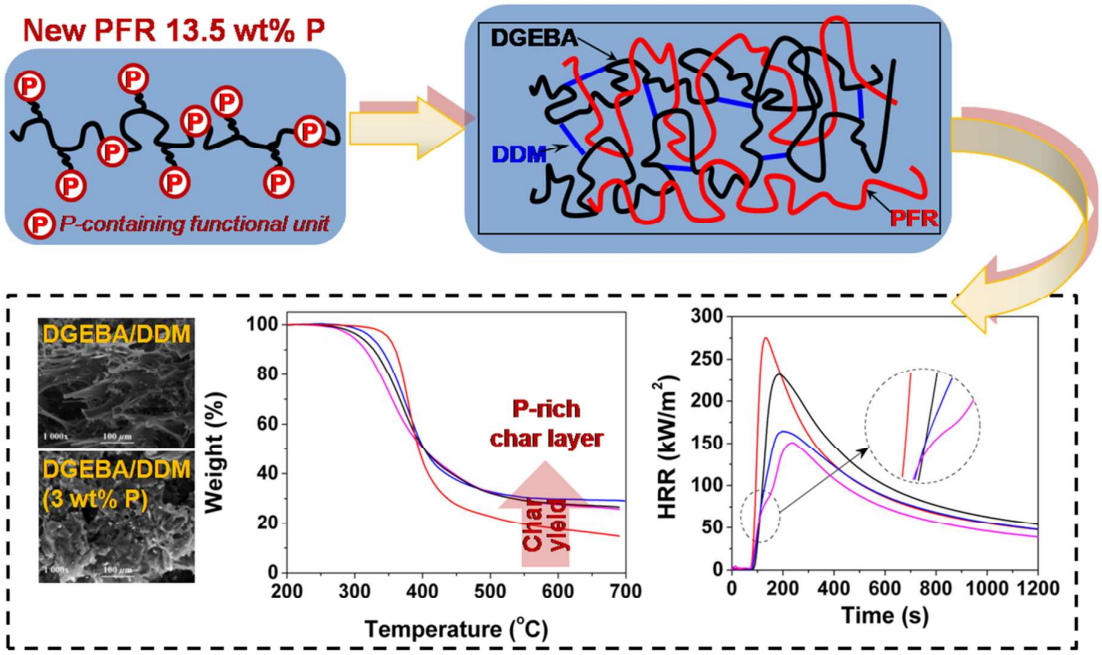

Textual Abstract

Commercial epoxy resin loaded with phosphorus flame retardant led to composites exhibiting remarkable improved flame retardancy and thermal stability.